In vivo mouse imaging using frequency domain optoacoustic tomography

Stephan Kellnberger¹, Nikolaos C. Deliolanis¹, Daniel Queirós¹, George Sergiadis², and Vasilis

Ntziachristos¹

¹ Chair for Biological Imaging, Technische Universität München & Helmholtz Zentrum München, Munich, Germany.

² Department of Electrical and Computer Engineering, Aristotle University, Thessaloniki, Greece.

Corresponding author: stephan.kellnberger@tum.de

Abstract: Frequency domain optoacoustics relates to stimulation of optoacoustic signals using intensity modulated continuous wave light instead of pulsed laser light employed in time domain optoacoustic imaging. We present a method to generate frequency domain tomographic images of optical absorbers and cross sectional *in-vivo* mouse images, showing the changes of optical absorption before and after injection of indocyanine green (ICG).

OCIS codes: 170.6960, 170.3880, 170.5220

1. Introduction

Implemented in the time domain, optoacoustic imaging usually employs nanosecond near-infrared (NIR) lasers at high energies (in the order of 10 - 100 mJ/optical pulse) to induce broadband acoustic responses of optical absorbers. Alternatively, optoacoustic signals can also be stimulated using intensity modulated light sources, i.e. high frequency modulated continuous wave (CW) lasers. Compared to time domain optoacoustic imaging (TD-OAI), frequency domain optoacoustic imaging (FD-OAI) offers more reliable and economic light sources and technically simpler implementations [1]. Lower energy levels and correspondingly lower signal to noise ratios (SNR) occurring in the frequency domain are counterbalanced by higher duty cycles.

Applications in frequency domain optoacoustic imaging so far focused on xy raster scanning of objects, inducing narrowband optoacoustic signals by means of an acousto-optic modulated Nd:YAG laser [1,2]. We present results obtained with a dedicated frequency domain scanner. Instead of horizontal line scanning of objects, our method achieves multi-projection acoustic signal acquisition, i.e. detection of optoacoustic responses at several angles relatively to the object. To retrieve the position of optical absorbers from the detector, we coherently process linearly induced optoacoustic signals. Cross sectional images are then reconstructed applying the filtered-back projection method, similar to time domain optoacoustic tomography [3].

2. The experimental FD-OAT scanner

The developed frequency domain optoacoustic tomography (FD-OAT) scanner is schematically depicted in Fig. 1. A function generator (Model 33210A, Agilent Technologies, Santa Clara, California, USA) drives a temperature stabilized diode laser (Omicron A350, Omicron-Laserage Laserprodukte GmbH, Rodgau-Dudenhofen, Germany). The emission wavelength of the diode laser is 808 nm with a peak power of 500 mW. For optoacoustic measurements, the function generator modulated the laser intensity with a frequency sweep from $f_{start} = 1$ MHz to $f_{stop} = 5$ MHz, achieving an excitation bandwidth of 4 MHz. Narrowband optoacoustic signals were detected using a focused ultrasound transducer (Model V382, central detection frequency: 3.5 MHz, focal distance: 3.81 cm, detection bandwidth: 76%, Olympus-NDT, Waltham, Massachusetts, USA) and subsequently pre-amplified employing a low-noise 65 dB amplification unit (Model: AU-1291, Miteq, Hauppage, New York, USA). A photodetector diode collected scattered light from the object. A trigger signal (MXG5181, Agilent Technologies, Santa Clara, California, USA) synchronized the data acquisition system, comprised of a digital phosphor oscilloscope (Model: DPO 7254, Tektronix Inc., Beaverton, Oregon, USA), and

Opto-Acoustic Methods and Applications, edited by Vasilis Ntziachristos, Charles P. Lin, Proc. of OSA Biomedical Optics-SPIE Vol. 8800, 88000A · © 2013 OSA-SPIE CCC code: 1605-7422/13/\$18 · doi: 10.1117/12.2032937

Proc. of OSA-SPIE Vol. 8800 88000A-1

the function generator modulating the CW laser.

Tomographic measurements were performed using a rotation stage (PR50PP, Newport Corporation, Irvine, California, USA) which allowed for simultaneous motion of the optical unit (i.e. the optical fiber and the photodetector) and the acoustic detector (i.e. the ultrasonic transducer). To collect a tomographic data set, optoacoustic responses were captured at 2° angles around the object. The total acquisition time per image was ~10 min. A dedicated code in MATLAB (Mathworks, Natick, Massachusetts, USA) was employed to control the positioning of the stage, the function generator, data acquisition and to post-process the recorded tomographic data.

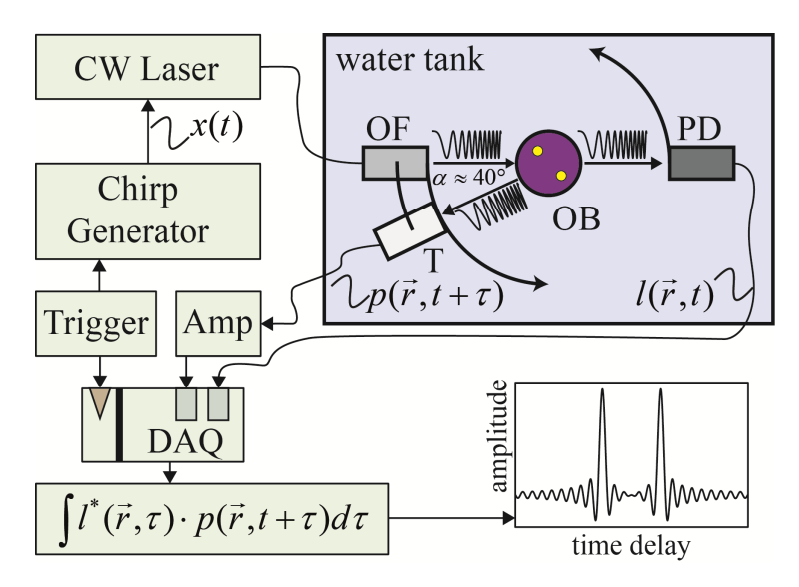


Figure 1. Schematic representation of the tomographic scanner used for frequency domain optoacoustic imaging (according to [4]). Intensity modulated laser chirps from a 808 nm CW laser illuminate the object (OB) using an optical fiber (OF). A data acquisition card (DAQ) detects simultaneously optoacoustic signals from the transducer (T) and reference chirp signals from the photodetector (PD). After cross correlation, the time delay of optical absorbers, i.e. the spatial distribution, can be resolved.

3. Results

To resolve radial distances of optoacoustic sources, time domain optoacoustic tomography relies on time-of-flight measurements defined by the trigger event (i.e. the laser pulse) and the propagation delay of emanating acoustic waves [5]. In frequency domain, acoustic signals are induced continuously over the time period the stimulating source is on; thus, the time-space relationship can be retrieved by cross correlating the optical chirp signal with the measured optoacoustic response. Similar approaches were proposed in radar/sonar systems [6], but are also applied in optoacoustic line scanning methods [1,2].

Modulating the laser with a linear frequency modulated signal (chirp)

$$x(t) = A\cos\left(2\pi f_0 t + \pi k t^2\right) \tag{1}$$

where f_0 is the initial frequency, A the amplitude and k the sweep rate, the spatial distribution of optical absorbers can be calculated using the cross correlation of the optical chirp signal and the optoacoustic response according to

$$cc(\vec{r},t) = \int_{-\infty}^{\infty} l^*(\vec{r},t) \cdot p(\vec{r},t+\tau) d\tau , \qquad (2)$$

where $l(\vec{r},t)$ relates to the reference signal and $p(\vec{r},t+\tau)$ corresponds to the measured optoacoustic signal.

To reconstruct tomographic images, we first performed the cross correlation for each projection and subsequently applied the filtered backprojection method to the processed data, similar to image reconstructions in time domain optoacoustic tomography [3].

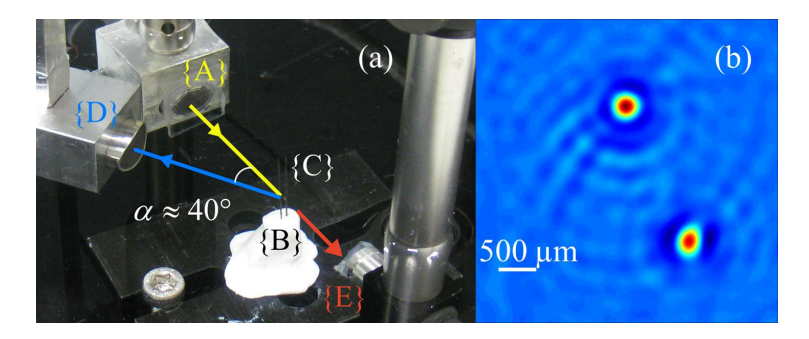


Figure 2. (a) Photograph of the experimental setup showing the optical laser beam $\{A\}$, the sample comprised of two graphite rods $\{B\}$ and $\{C\}$, the acoustic detector $\{D\}$ and the photodetector $\{E\}$. (b) FD-OAT reconstruction of the graphite objects (according to [4]).

The experimental frequency domain optoacoustic scanner is shown in Fig. 2(a). The objects, consisting of optically absorbing graphite rods, exhibited a diameter of 0.35 mm and were located in the center of the imaging tank, placed 2 mm apart. The corresponding optoacoustic cross sectional image is shown in Fig. 2(b), displaying the orientation of absorbers in the imaging plane.

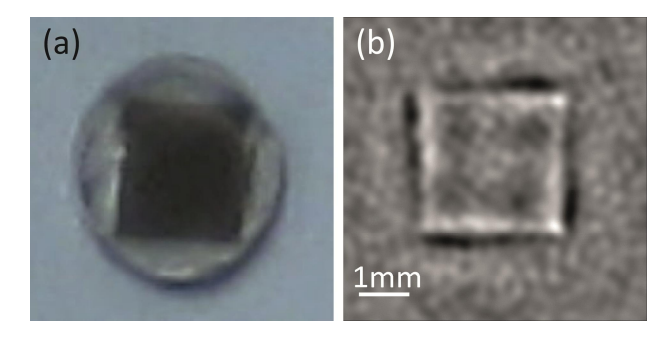


Figure 3. Phantom imaging (according to [4]). (a) Photograph of clear agar phantom 1, containing a 2 cm-1 rectangular insertion. (b) FD-OAT image reconstruction of phantom 1.

In a next step we examined the performance of the frequency domain scanner on clear agar phantoms with defined optical absorption inclusions. Phantom 1 contained a rectangular insertion of India Ink with an absorption coefficient of 2 cm⁻¹. Figure 3 depicts a photograph of the phantom with the corresponding reconstruction of cross correlated signals over 180 projections, shown in Fig. 3b.

Furthermore, we imaged a second phantom which exhibited a more complex geometry compared to phantom 1. The photograph of phantom 2 in Fig. 4 shows the layout of the hexangular 2 cm⁻¹ insertion. The reconstruction of cross correlated optoacoustic signals clearly reveals shape and size congruence to the picture.

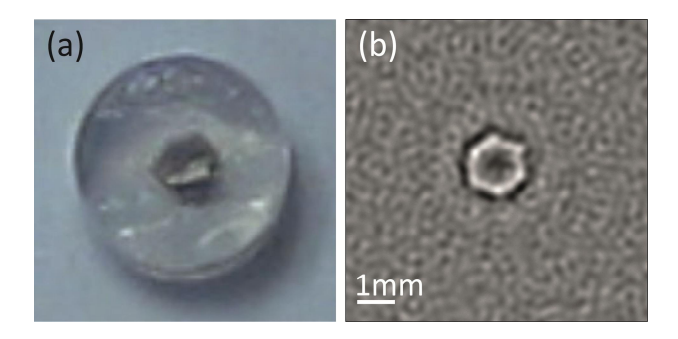


Figure 4. Phantom imaging (according to [4]). (a) Photograph of clear agar phantom 2, containing a 2 cm-1 hexangular insertion. (b) Corresponding FD-OAT image reconstruction of phantom 2.

Finally, we investigated the performance of the FD-OAT scanner in *in vivo* imaging. Therefore, we prepared a Balb/c female mouse for FD optoacoustic scanning. The mouse tail was immobilized using a custom made mouse holder and imaged at 40 mm from the distal end. Following the initial tomographic measurement, we subcutaneously injected 130 nmol of Indocyanine green (ICG) in the mouse tail using a catheter. Due to the acquisition time of 10 min/image and to compensate for clearance of ICG from the blood stream, we initialized a second injection of 100 nmol of ICG after ~ 4 minutes from the initial administration. To evaluate the reconstructed images, we cryosliced and photographed the imaged region of the mouse tail. Figure 5 shows frequency domain optoacoustic images of the mouse tail. Compared to the *ex vivo* cryosections taken at a similar height, there is exact congruence between the blood vessels highlighted in the FD-OAT image and the anatomical photograph of the mouse tail. The twofold optoacoustic signal increase in Fig. 5(b) relates to the higher optical absorption owing to contrast enhancing ICG, resulting in a SNR of 49.6 dB. Clearance of ICG due to the long acquisition time engenders a signal drop, shown in the post ICG measurement in Fig. 5(c).

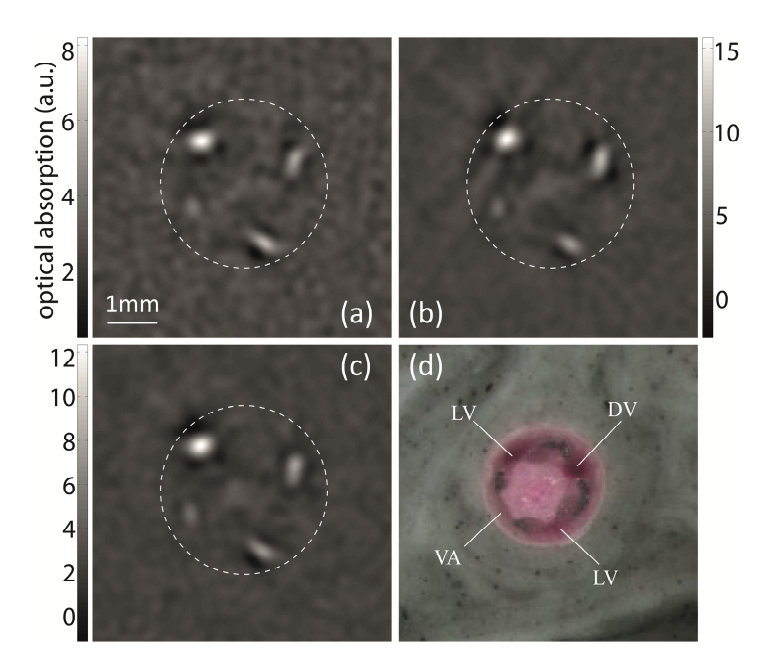


Figure 5. In vivo Frequency domain optoacoustic imaging (according to [4]). (a) Tomographic image of the mouse tail prior ICG injection. (b) Mouse tail cross section during injection of ICG. (c) FD-OAT image ~10 min after ICG injection. (d) *ex vivo* cryoslice of the imaged mouse tail (VA – ventral caudal artery, LV – lateral caudal veins, DV – dorsal caudal vein; tail surface is approximated by dashed lines).

4. Conclusion

In conclusion, we presented a method capable of recording and reconstructing tomographic optoacoustic images using intensity modulated CW lasers. Compared to frequency domain optoacoustic imaging using linear scanning, the tomographic approach allows for higher SNR and spatial resolution due to the higher effective aperture of the tomographic approach, enabling diffraction limited imaging resolution. The performance of the developed scanner was demonstrated on phantoms consisting of solid and soft tissue and *in vivo*, showing dynamically absorption changes in a mouse prior, during and after administration of ICG. Compared to time domain implementations, the FD-OAT scanner has the potential to facilitate technically simpler and cost-effective technology. Further investigations will focus on multispectral illumination of objects using an array of CW diode lasers at different wavelengths for simultaneous stimulation of optical responses.

5. References

- [1] S. A. Telenkov and A. Mandelis, "Fourier-domain biophotoacoustic subsurface depth selective amplitude and phase imaging of turbid phantoms and biological tissue," *J. Biomed. Opt.* **11**, 044006 (2006).
- [2] S. A. Telenkov, A. Mandelis, B. Lashkari, and M. Forcht, "Frequency-domain photothermoacoustics: Alternative imaging modality of biological tissues," *J. Appl. Phys.* **105**, 102029 (2009).
- [3] R. Ma, A. Taruttis, V. Ntziachristos, and D. Razansky, "Multispectral optoacoustic tomography (MSOT) scanner for whole-body small animal imaging," *Opt. Express* 17, 21414 (2009).
- [4] S. Kellnberger, N. C. Deliolanis, D. Queiros, G. Sergiadis, and V. Ntziachristos, "In vivo frequency domain optoacoustic tomography," Opt. Lett. 37, 3423 (2012).
- [5] D. Razansky, C. Vinegoni, and V. Ntziachristos, "Multispectral photoacoustic imaging of fluorochromes in small animals," *Opt. Lett.* **32**, 2891 (2007).
- [6] M. I. Skolnik, Radar Handbook, 3rd ed. (McGraw Hill. 2008).